15 March 1999

ELSEVIER

Optics Communications 161 (1999) 297–309

OPTICS COMMUNICATIONS

Full length article

Non-destructive optical characterization of photovoltaic modules by an integrating sphere. Part I: Mono-Si modules

Antonio Parretta *, Angelo Sarno, Haruna Yakubu [1]

ENEA Centro Ricerche, Località Granatello, C.P. 32, I-80055 Portici (Na), Italy

Received 3 August 1998; revised 19 January 1999; accepted 21 January 1999

Abstract

The optical reflectance properties of commercial and prototype monocrystalline silicon photovoltaic (PV) modules were characterized in a non-destructive way by using an apparatus equipped with a 40-cm diameter integrating sphere. The modules showed different reflectance properties in relation to their different fabrication technologies. The lowest reflectance values, about 4% at $\lambda = 632.8$ nm and near normal incidence, were obtained from different front structures, all containing an anti-reflection coating (ARC). Modules without ARC, on the contrary, showed total reflectances in the 6–9% interval. The total and diffuse reflectances were also measured as a function of the incident angle of a He–Ne laser beam at a fixed azimuth orientation of the incident plane. The modules with flat glass tops showed flat reflectance curves from 10° to 40°, whereas those with textured glass tops showed flat reflectance curves from 10° to 50°. In order to compare the different total reflectance curves, we introduced a 'light collection factor' for inclined light, f_{IL}, with respect to the normal incidence. We found a certain correlation between the light collection factor and the front structure of the modules. In particular, we established that front covers with textured glass tops collect the inclined light slightly better with respect to the front covers with flat glass tops, and then are expected also to collect slightly better the diffuse light from the sky hemisphere. Finally we found that the front covers of the mono-Si modules, as far as conditions relative to normal incidence are considered, can be optically modeled as homogeneous dielectrics with refractive index higher than that of glass (1.5) and in the interval 2.5–3.0. The precise value depends on the particular structure of the module's front cover.

PACS: 07.60.Hv; 42.85.Fe; 84.60.Jt

Keywords: PV modules; Optical losses; Integrating spheres

1. Introduction

Solar photovoltaic (PV) modules play a significant role in the quest to develop new energy sources that are both abundant and environmentally friendly. For the optimization and effective operation of solar modules, their output dependence on real operating conditions must be studied [1]. Detailed studies [2] reveal that real operating efficiencies are not always equal to the nominal efficiencies determined at Standard Test Conditions (STC) [3]: (i) normal incidence and (ii) unpolarized radiation; (iii) 1000 W/m^2 irradiance level; (iv) AM1.5G light spectrum and (v) 25°C temperature. The corresponding five parameters – (i) incident angle of the light beam, (ii) polarization of the light, (iii) irradiation level, (iv) spectrum of the light and (v) module's temperature – together contribute to determining the real efficiency, and hence the real power, of the PV module in outdoor operation. The angle of incidence of the light is, besides the module's temperature and the

* Corresponding author. E-mail: parretta@epoca1.portici.enea.it

[1] Permanent address: Department of Physics, University of Cape Coast, Cape Coast, Ghana.

0030-4018/99/$ - see front matter
PII: S0030-4018(99)00037-1

irradiation level, an important parameter affecting the efficiency of the module [4,5]. When the light is incident on the module's surface at an angle different from the normal, the reflection of the module, in general, increases and the consequence is that less light arrives at the semiconductor. Also the absorbance of light from the glass/EVA cover is expected to change by changing the incident angle. The loss corresponding to the reflection and absorption of light at the module's front cover, in terms of efficiency and power, is called 'optical loss'. The 'optical loss', therefore, is a relative concept, when it is referred to the STC conditions. It is zero at an incidence normal to the module's surface ($\theta = 0°$) and, in general, increases when increasing the incident angle θ.

The study of the optical reflectance properties of PV devices, both absolute and relative to normal incidence, is an important step for determining their optical losses. The knowledge of the absolute reflectance helps in projecting modules with lower absolute optical losses thus saving more energy. Also, the knowledge of the reflectance, relative to the normal incidence, helps in selecting modules more suitable for specific outdoor conditions, as those with a high content of diffuse light (northern Europe) or those with high angles of incidence of the direct component of the sunlight (façades).

The optical losses of modules, relative to STC, could be studied also by measuring their short circuit current at different incident angles of the light. This method is the most direct one, as it allows to measure the combined effect of reflectance and absorbance in the same measurement. It requires, however, an expensive experimental apparatus consisting of a light source highly stable and sufficiently large to illuminate, homogeneously, the entire module's surface.

Our 'integrating sphere' method is an alternative to that of the current, but substantial differences exist between the two. Our method allows to measure the 'local' reflectance, not the average; it gives both the 'absolute' and 'relative' loss, whereas the current method gives only the relative loss; last and more important is the fact that our method can be applied to any 'passive' substrate, not necessarily a PV device.

This paper is devoted to the optical characterization (total and diffuse reflectance measurements) of mono-Si PV modules, in order to find a correlation between the optical reflectance properties and the structure of the modules. The light reflection does not exhaust the optical loss, as there is also absorption of light inside the front cover to be considered; nevertheless, it is the main mechanism of loss of light in the module, particularly at high incidence angles. The measurement of the absorbance loss, on the other hand, is a very difficult task, as it depends on the light path inside the cover and thus on the light trapping properties of encapsulation. An independent measurement of absorbance on the glass cover sheet alone is possible, but it could not reproduce the light trapping mechanism acting in the real PV device. In this paper we present only reflectance results and are able to estimate only the optical losses due to reflection. Neglecting the absorption of light at the module's front cover brings a little underestimation of the optical losses and this is to be considered when comparing our results with those obtained by the direct photocurrent method.

The calculation of the 'energy loss', corresponding to the optical loss derived from the reflectance data, is not the purpose of the present paper. It can be performed, for example, following the method outlined by us in previous papers [6,7].

Until recently, even though some work had been done on optical loss measurements [4,5,8], much of the work had been devoted to theoretical simulations [5,6,9]. In Ref. [4] the authors measured the relative transmittance of solar modules and compared their results with simulated calculations. The authors of Refs. [6,7] reported that the optical losses related to the reflection of the diffuse and direct sunlight components are about 20% of the total energetic loss. By simulation, it is also shown that losses due to reflection account for 6–10% of the decrease in current yield in solar PV modules [5]. This wide range of data calls for more experimental work to better investigate the sources of optical losses and, possibly, for models which could be of practical and simple use when the energetic loss of an installed module has to be estimated.

Although there are several applicable test methods (spectrophotometers) employed for determining the optical properties of materials, they are generally used for 'ad hoc' prepared samples. For unusual size samples, like PV modules and large glass sheets, and for angle dependent measurements, conventional spectrophotometric techniques cannot be used. Integrating spheres are widely used to measure the reflectance and transmittance of optical samples [10]. The use of integrating spheres for carrying out optical measurements presents several advantages, namely, their non-destructive nature, no preliminary sample preparation and easy sample handling.

Our newly developed integrating sphere has been projected looking to applications in the wide field of solar energy. By using it, we have found that the absolute reflectance at normal incidence reaches the limit imposed by the Fresnel equations, about 4% for a flat air/glass interface, in the most recent mono-Si modules. We have also investigated the optical behaviour of the modules to non-normal light beams. Previous theoretical studies have shown that the transmittance of the glass/EVA/ARC top structure at different incidence angles is dominated by the air/glass interface [11]. Our results confirm these achievements. Our model for the PV module, however, is based on the application of the Fresnel equations to a general air/dielectric interface, with the dielectric having an equivalent refractive index n_{eq}, not necessarily equal to that of glass (1.5) [6,7], and to be optimized by optical measurements. We have made an experimental verification

of the different models proposed by directly measuring the reflectance of different mono-Si modules at different incident angles. These measurements are intrinsically difficult to carry out because of the presence of the grid on the cells' surface. The glass/EVA/grid structure shows, in fact, reflectivities as high as 70%. To overcome this problem, a laser beam ($\lambda = 632.8$ nm), focused between two grid fingers of the cells, has been used. The azimuth orientation of the incident plane of the laser beam has been the same as that of the sun's direct component, averaged over a year, if the module were installed at a tilt angle equal to the latitude and oriented towards the South (for installations in the northern hemisphere). Our reflectance results, therefore, can be applied to the outdoor optical behaviour of the module with respect to the direct component of the sun. For modules with an isotropic surface (flat-Si surface), the same results can also be applied to the diffuse radiation.

We have found that the collection of inclined light beams is slightly affected by the structure of the module's front cover and that the most effective parameter, in this regard, is the roughness of the top surface of the glass. We have also found that modules with a flat top glass surface and with ARC can be modeled as homogeneous dielectrics with an equivalent refractive index $n_{eq} \approx 2.5$, whereas modules with a flat top glass surface without ARC, and modules with a textured top glass surface, can be modeled as dielectrics with $n_{eq} \approx 3.0$. This distinction, however, is not so precise, as no experimental curve perfectly matches the theoretical ones, due to the fact that the module, in reality, is not a homogeneous dielectric. The study of the reflectance curves has allowed us to confirm the approach used in our previous investigations [8,9] – the possibility of finding a simple optical model for the modules – that is, dielectrics with an equivalent refractive index different from that of glass ($n = 1.5$). Previous investigations made by us and other authors [4,8,11] brought to the conclusion that the module can be simply modeled as glass ($n = 1.5$), with respect to its relative transmittance properties. We have found, indeed, that the flat glass plus ARC modules show $n_{eq} \approx 2.5$, which is not too different from $n_{eq} \approx 1.5$ (see Fig. 14) and thus our results agree with those of other authors if this particular type of module's structure is considered.

2. Experimental

2.1. The optical apparatus

The optical apparatus, suitable for a wide variety of optical measurements on materials and devices used in the

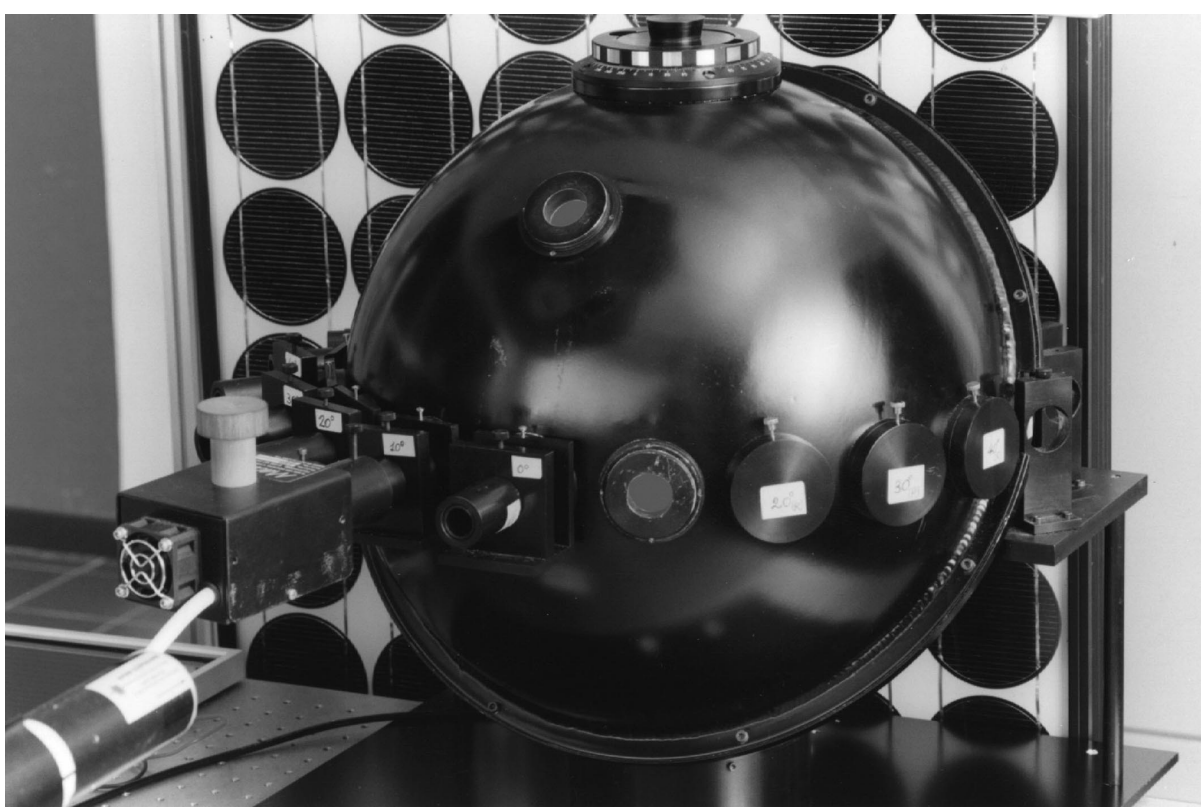

Fig. 1. Picture of the ROSE optical apparatus.

solar energy field, has been patented [12] and is described in more detail elsewhere [13,14]. Fig. 1 shows a picture of the apparatus in the configuration for reflectance measurements on PV modules. Fig. 2a and b are schematic representations of the lateral and top views of the apparatus. The apparatus, also called ROSE (Reflectometer for Optical measurements in Solar Energy), was built by MACAM Photometrics. It includes an integrating sphere, an external source of light and a detector/radiometer measurement system. The integrating sphere (s), made of aluminum, has a 40-cm diameter and is internally coated with $BaSO_4$. It is provided with several ports (i) for the input of light, corresponding to different incident angles of 0°, 10°, 20°, . . . , 70°, distributed along the equatorial line of the sphere. Seven specular windows (a) allow to intercept the specular beam reflected from the module. They are closed with $BaSO_4$-coated, white caps when measuring the total reflectance and with a black absorber when measuring the diffuse reflectance. The light source (l) can be of any kind, but we used a highly stable He–Ne laser and a stabilized QTH lamp to limit the instability of the light intensity during the measurements. The window (w) has a maximum diameter of 7.5 cm and is provided to face the sample's testing area towards the interior of the sphere. The sample (m), when it is a module or a large glass sheet, is fixed on the frame (t) and sustained by the trolley (b), when it is a solar cell, it is fixed directly on the window (w). The beam position is regulated by viewing the test area through the view port (o). The irradiance inside the sphere, produced by the reflected light, is measured by a silicon photodiode which serves as the detector (d) and is connected to the radiometer (r). For spectral measurements, a filter (f) is mounted in front of the detector (d) or a monochromator is installed between the light source and the sphere. Reference measurements were made on a Perkin Elmer Lambda 9 spectrophotometer by using Labsphere Spectralon standards of reflectance.

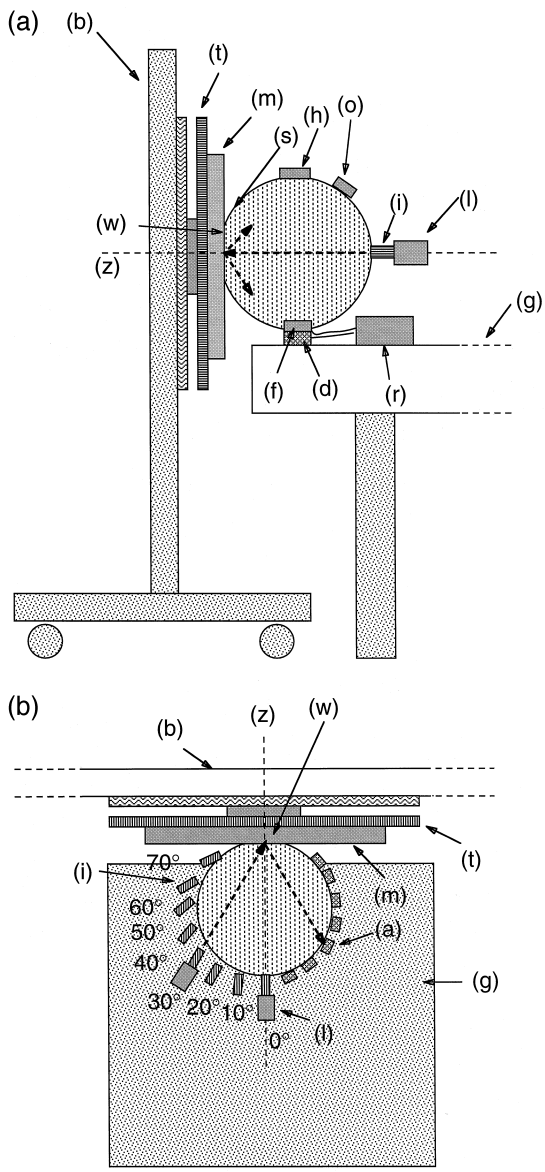

Fig. 2. (a) Side view of the ROSE optical apparatus. (b) Top view of the ROSE optical apparatus.

2.2. Samples

The characterized samples were commercial and prototype monocrystalline silicon modules. The modules were classified into six categories (from A to F) depending on the fabrication technology of the front structure of the cells (see Table 1). The six categories were defined without taking into account the roughness of the glass/EVA interface because of lack of information. However, information on the glass/EVA interface, where available, is reported in Table 2. Table 1 shows the type of specular spot of the reflected beam, observed on the specular port inside the sphere. A dot-like spot was observed from the modules with flat glass top surfaces, whereas a fractal-like spot was observed on modules with textured glass top surfaces. The modules whose glass sheet is flat on the top and textured on the bottom showed again a dot-like specular spot. Table 2 shows all the tested modules, their year of fabrication and their category. The texturization of the encapsulated silicon wafers was easily checked by focusing the laser beam onto their surface at near-normal incidence: a peculiar figure due to the small square pyramids can be clearly seen on the surface of the textured-Si module (see Fig. 3). Some of the modules of Table 2 were manufactured in a non-conventional way: module 1 (BP Solar) was made with laser grooved buried grid (LGBG) solar cells [15], module 14 (ENEA/Helios/CNR-Lamel) with solar cells fabricated by using an ion implantation method and module 17 (SNES) has a luminescent front glass sheet to drift

Table 1
Categories of the tested mono-Si modules, in relation to their front structure. The reference to the glass is made only for the top surface. The table contains also the type of spot of the specularly reflected beam and the average equivalent refractive index, n_{eq}

Category	Front structure	Reflectance spot	n_{eq}
A	Flat-glass/text-Si	dot	≈ 3.0
B	Flat-glass/ARC/text-Si	dot	≈ 2.5
C	Flat-glass/ARC/flat-Si	dot	≈ 2.5
D	Text-glass/text-Si	fractal	≈ 3.0
E	Text-glass/ARC/flat-Si	fractal	≈ 3.0
F	Text-glass/ARC/text-Si	fractal	≈ 3.0

the sun's spectrum towards spectral regions of higher response.

2.3. Reflectance measurements

A coherent, 1-mW, linearly polarized, He–Ne laser operating at $\lambda = 632.8$ nm and a 150 W QTH lamp were used as light sources in the present paper. Due to the linear polarization of the laser, two series of measurements at two orthogonal orientations were necessary to obtain, on the average, the same reflectance values expected for unpolarized light. Apart from the spectral measurements, where the QTH lamp was used, all the other reflectance measurements were carried out by focusing the laser beam between two finger lines of the solar cell, hence measuring the reflectance of only the optically active area of the encapsulated solar cell [12,13]. The near-normal incidence reflectance measurements were made at 10°, since total reflectance measurements at 0° were not possible. In fact, the specular beam exits from the 0° port and cannot be measured when a beam splitter is not used. The angular measurements were therefore carried out from 10° to 70°, maintaining the incidence plane of the laser beam orthogonal to one axis of the module (one of the two that is generally aligned to the North–South direction in outdoor installations). The angular movement of the laser beam corresponds, on the average, to that of the sun's direct light when the module is installed at a latitude tilt and oriented towards the South (northern hemisphere). The azimuth orientation of the laser beam is described in Fig. 4. Fig. 5 illustrates how the laser beam spot is viewed on

Table 2
List of the tested mono-Si modules. It shows the year of fabrication, the category (see also Table 1), the total reflectance, the absolute diffuse reflectance and the relative diffuse reflectance

N	Type	Year	Category	Glass back surface	R_{tot} (%)	R_{diff} (%)	R_{diff}^{rel} (%)
1	BP Solar BP585	1994/1995	B	textured	4.3 ± 0.2	0.3 ± 0.2	8 ± 4
2	Italsolar 36MSCE	1988	A	flat	7.1 ± 0.2	3.3 ± 0.2	46 ± 4
3	Italsolar 36MSCE	1988	A	flat	6.2 ± 0.2	2.7 ± 0.1	$43. \pm 3$
4	Ansaldo, prototype	1986	E	textured	5.3 ± 0.4	1.7 ± 0.2	31 ± 6
5	Helios HT5563	1988	A	flat	6.6 ± 0.2	3.1 ± 0.2	46 ± 4
6	Helios B5033	1988/1989	D	textured	6.2 ± 0.1	3.5 ± 0.2	57 ± 3
7	AEG MQ10	1989	C	?	4.1 ± 0.1	0.2 ± 0.1	4 ± 1
8	Pragma S24P3	1985	E	textured	7.7 ± 0.1	4.3 ± 0.1	56 ± 3
9	Helios S347	1991	D	textured	6.3 ± 0.1	2.9 ± 0.1	46 ± 3
10	Helios S161	1991	D	textured	6.3 ± 0.2	2.9 ± 0.2	47 ± 4
11	Helios H50	1993/1994	D	textured	8.4 ± 0.6	4.9 ± 0.1	58 ± 6
12	Ansaldo AP38HD	1986	E	textured	4.9 ± 0.6	1.6 ± 0.2	33 ± 7
13	Arco Solar M55	1990/1991	F	?	5.0 ± 0.5	1.7 ± 0.3	33 ± 8
14	ENEA/HT/Lamel	1986	D	textured	6.2 ± 0.3	3.4 ± 0.2	55 ± 6
15	Helios, prototype	1988	D	textured	7.4 ± 0.3	4.5 ± 0.1	61 ± 4
16	Ansaldo, prototype	1986	E	textured	3.9 ± 0.2	0.6 ± 0.1	14 ± 3
17	SNES S22.12	1983	B	?	3.7 ± 0.2	0.5 ± 0.2	13 ± 6
18	Italsolar 36MSCE	1988	A	flat	6.9 ± 0.2	3.1 ± 0.1	45 ± 3
19	Italsolar 36MSCE	1988	A	flat	6.6 ± 0.1	2.5 ± 0.1	39 ± 2
20	Italsolar 36MSCE	1988	A	flat	6.0 ± 0.1	2.9 ± 0.1	49 ± 3
21	Italsolar 36MSCE	1988	A	flat	6.4 ± 0.1	2.8 ± 0.1	45 ± 3

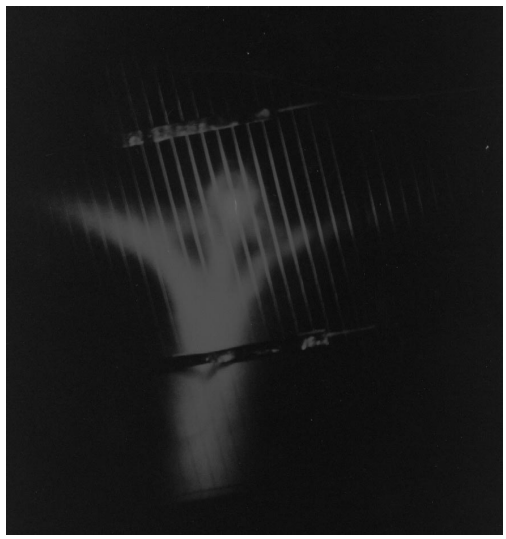

Fig. 3. Reflection of the laser beam by a textured-Si encapsulated cell.

the solar cell; even at high incidence angles, the laser spot remains confined between two finger lines. Angularly dependent measurements were made on most of the modules. For modules with dot-like specular spots, both the total and the diffuse reflectances at the different angles were measured. Only the total reflectance as a function of the incidence angle was measured for modules with fractal-like specular spots.

Spectral measurements on the modules were carried out by using the QTH lamp at a fixed angle of 10°. Two filters, one low λ pass and the other high λ pass, were installed in front of the detector for each measurement, in order to have a bandwidth of ≈ 100 nm. The light spot on the module's surface from the QTH source was circular of 1-cm diameter and illuminated both the optically active area of the solar cell and the grid (see Fig. 6). To correct the effect of the grid on the reflectance measurements, we used a procedure that is outlined in Section 2.4.

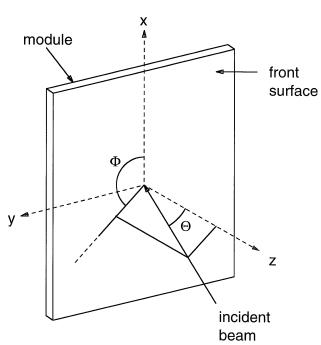

Fig. 4. Definition of incidence angle (θ) and azimuth angle (ϕ) of the light beam.

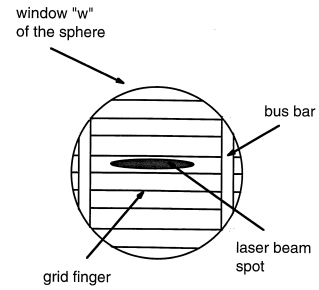

Fig. 5. Picture of the solar cell as viewed from the window 'w' inside the sphere, when the laser beam is incident on the cell surface at a high incidence angle. The beam spot is focused between two finger lines.

2.4. Grid effects on the reflectance measurements

To obtain the reflectance of the optically active area, R_{oa}, of the module, that is that which transmits the light to the active layers of the device, some corrective formulae have to be applied to the measured reflectance [13]. The reflectance R_{oa}, if we neglect here its dependence on ϕ (the azimuth angle of the incident plane of light) in textured modules, can be expressed as:

$$R_{oa}(\theta) = \left[\underline{R}(\theta) - R_g(\theta)S_g\right]/S_{oa}, \tag{1}$$

where θ is the incidence angle of the light beam, $\underline{R}(\theta)$ is the measured reflectance on the fine grid area, $R_g(\theta)$ is the grid reflectance, $S_{ill} = S_g + S_{oa} = 1$ is the illuminated area, S_{oa} is the optically active fraction of S_{ill} and S_g is the grid fraction of S_{ill}.

S_g and S_{oa} can be easily found by measuring the fingers width and distance with an optical microscope with a long focal length. The grid reflectance $R_g(\theta)$ can be derived experimentally by a single reflectance measurement with the light spot centered on the bus bar of the cell, when the bus bar metal is the same as that of the grid-finger metal. Putting realistically $R_g(\theta) \approx R_g(0°)$, we obtain

$$R_g(0°) \approx \left[\underline{R}'(0°)\left(\pi d^2/4\right) - \underline{R}(0°)\left(\pi d^2/4 - sd\right)\right] /(sd), \tag{2}$$

where $\underline{R}'(0°)$ is the measured reflectance on the bus bar area, $\underline{R}(0°)$ is the measured reflectance on the fine grid area, d is the light spot diameter and s is the bus bar

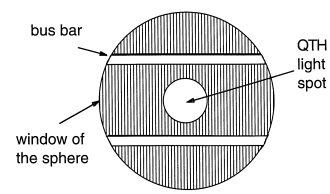

Fig. 6. Picture of the solar cell as viewed from the window 'w' inside the sphere, when the QTH beam is incident on the cell surface at 10° incidence angle. The beam spot illuminates both the fingers and the silicon surface.

width. It is sufficient to make two measurements, one on the fine grid area, $\underline{R}(\theta)$, and one directly on the bus bar, $\underline{R}'(0°)$, to obtain the reflectance of the optically active area of the solar cell in mono-Si or poly-Si modules. As an alternative to Eq. (2), $R_g(0°)$ can be derived theoretically by optically modeling the glass/EVA/metal structure. For integrated modules (a-Si, CIS), a single measurement with the light beam between two adjacent laser scribed lines is sufficient to give $R_{oa}(\theta)$.

The above described measurements can be used to know the absolute transmittance of the optically active area, $T_{oa}(\theta)$, if the absorbance of the glass cover, $A_{oa}(\theta)$, is known [13]:

$$T_{oa}(\theta) = \left\{1 - \underline{R}(\theta) - S_g\left[1 - R_g(0°)\right] - \left(1 - S_g\right) A_{oa}(\theta)\right\} / \left[1 - S_g\right]. \quad (3)$$

The 'relative transmittance' of the front cover of the module with respect to STC, $T_{oa}(\theta)/T_{oa}(0°)$, can be calculated by Eq. (3). It is a fundamental quantity in the evaluation of the optical losses of a PV module under outdoor conditions [6,7]. The quantity $A_{oa}(\theta)$ can be derived by reflectance and transmittance measurements on a glass sheet equal to that used in front of the module or even directly on the module itself if it is made of a glass/EVA/glass cover structure. In this case, a small error will be made as a consequence of the fact that the back glass sheet does not have exactly the same optical properties as the front glass. As it is known, the front glass sheet has to be highly transparent to light and thus is made with a low iron content, whereas the back glass sheet is optimized for its mechanical properties [16].

3. Results and discussion

3.1. Reflectance measurements at $\lambda = 632.8$ nm

The directional/hemispherical total reflectance [17], indicated here as R_{tot}, at 10° incidence angle and $\lambda = 632.8$ nm, for different types of commercial and prototype mono-Si PV modules, is reported in Table 2. From the table, it can be seen that the modules without ARC and module 8 have R_{tot} values in the 6–9% interval, whereas those with ARC have R_{tot} values in the 4–6% interval, independent of the module's front structure. The presence of ARC, therefore, as is expected, is fundamental in reducing the total reflectance of the module at near-normal incidence. The lowest reflectances at 10° were obtained with a module of category E and the special module 17. Also modules of categories B and C showed very low values of R_{tot}. By considering the year of fabrication of the modules and their total reflectance in Table 2, it is not easy to find a correlation between these two quantities. Most of the tested modules were fabricated in the late eighties, and hence it is not possible to follow the evolution of the fabrication technology by the actual optical measurements.

Besides the total reflectance, Table 2 also shows the absolute diffuse reflectance (R_{diff}) and the diffuse reflectance relative to the total (R_{diff}^{rel}) in percentage. Fig. 7 correlates the diffuse and total reflectances values of Table 2. An approximately linear correlation between R_{diff} and R_{tot}, independent of the module category, is observed, with an intercept of about 3.5% on the R_{tot} axis:

$$R_{tot} \approx 3.5 + R_{diff}\,(\%). \quad (4)$$

It appears evident that the smallest values of R_{tot} are attained when values of R_{diff} are near zero. On one hand, it seems reasonable to attribute the significance of a specular reflectance to the intercept on the R_{tot} axis of the R_{diff} versus R_{tot} best-fit plot. On the other hand, the intercept roughly corresponds to the reflectance foreseen by the Fresnel equations for an air/glass interface when n(glass) ≈ 1.5. To better investigate this fact, we plotted separately the reflectance points relative to the modules with flat glass top surface (see Fig. 8a) from those with textured glass top surface (see Fig. 8b). In the first case we obtained:

$$R_{tot} \approx 3.9 + 1.1 R_{diff}\,(\%), \quad (4a)$$

whereas in the second case we obtained:

$$R_{tot} \approx 3.3 + 1.0 R_{diff}\,(\%). \quad (4b)$$

From Eqs. (4a) and (4b) and from what we expect to have for an air/flat-glass interface, it is obvious that the specular reflection arises mainly from the air/glass interface and that the diffuse reflection arises mainly from the internal interfaces (Glass/EVA, EVA/ARC, ARC/Si or Glass/EVA, EVA/Si). We can write, therefore:

$$R_{tot} \approx R(\text{air/glass}) + R_{diff}. \quad (4c)$$

Fig. 9a and b illustrate how, in our opinion, the light could be reflected by two types of structures: flat/text-glass/EVA/ARC/text-Si and text/text-glass/EVA/ARC/text-Si, respectively. The first structure produced a

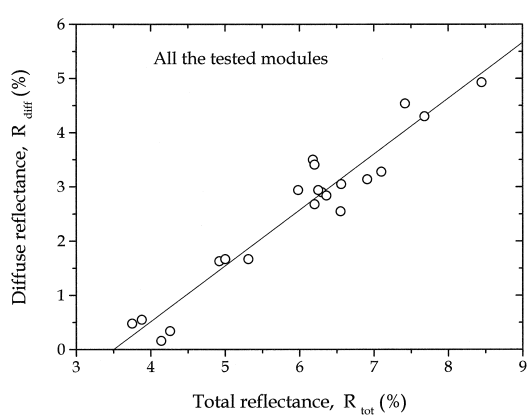

Fig. 7. Absolute diffuse reflectance versus the total reflectance for all the tested mono-Si modules. A clear correlation exists between the two quantities.

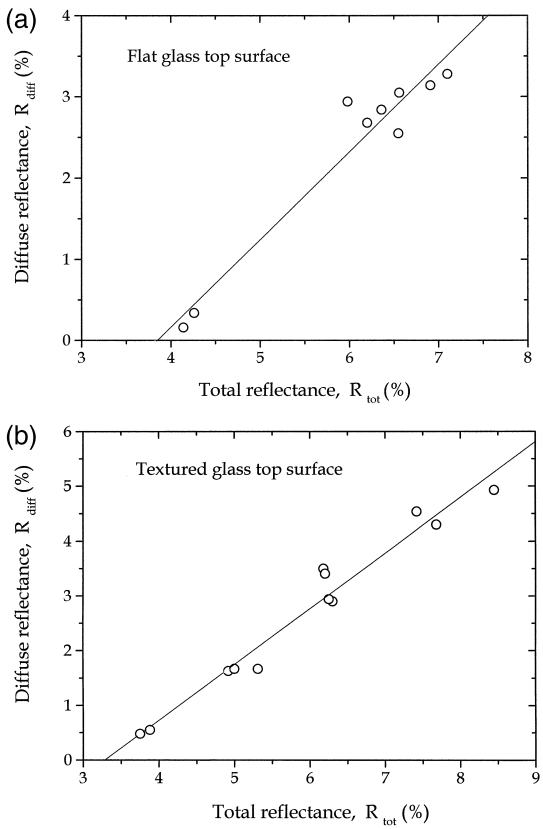

Fig. 8. (a) Absolute diffuse reflectance versus the total reflectance for modules with flat glass top surfaces. (b) Absolute diffuse reflectance versus the total reflectance for modules with textured glass top surfaces.

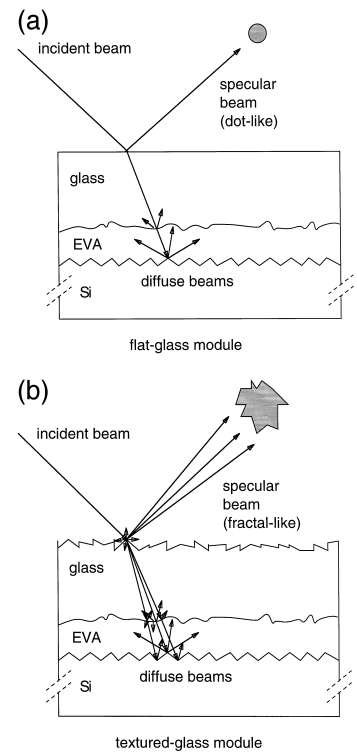

Fig. 9. (a) Schematic representation of the reflection process with a flat-glass module (dot-like reflected spot). (b) Schematic representation of the reflection process with a textured-glass module (fractal-like reflected spot).

dot-like specular reflected spot and the second a fractal-like one. The dot-like spots were measured by opening the specular window corresponding to the 10° port (see Fig. 2b) and then extracting a cone of light as large as 3 msr. The fractal-like spots, being larger than the specular window corresponding to the 10° port, were measured by inserting a cylindrical tube (white on the outside and black on the inside) into the sphere from the 10° specular window in order to 'capture' the specular beam nearer to the surface of the module (see Fig. 10). The solid angle at which the specular beam was intercepted in this case was about 12 msr. The reflection of the air/textured-glass interface results to be about 3–3.5%, which is a little smaller than that obtained for the air/flat-glass interface, of about 4%. A glass sheet textured on the front, therefore, seems to reduce the ultimate total reflectance of the module. It is clear from Eq. (4c) that the specular reflection from the bottom glass/EVA interface is negligible for both flat and textured interfaces. The BP585 module, as an example, has a flat glass top and a textured glass bottom (see Table 2), but shows a dot-like specular spot like the modules with flat surfaces on both sides of the glass sheet. This reveals a good optical matching between glass and EVA on both flat and textured glass bottom surfaces.

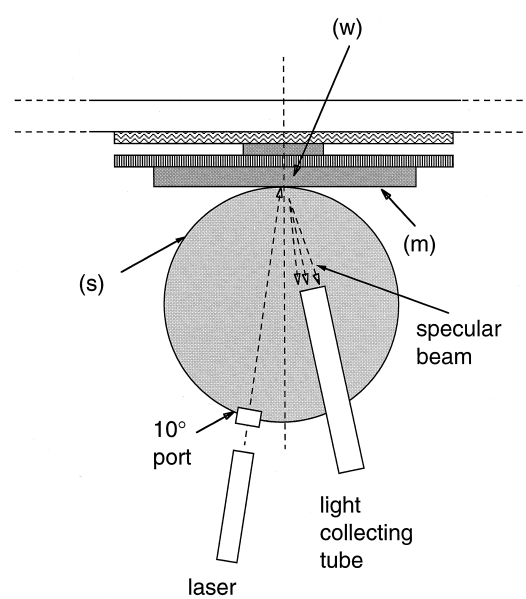

Fig. 10. Configuration of the sphere when measuring the diffuse reflectance of a textured-glass module.

The total reflection curves, $R_{tot}(\theta)$, as a function of the incidence angle between 10° and 70°, are shown in Fig. 11a for some modules with flat top surface and in Fig. 11b for some modules with textured top surface. R_{tot} generally maintains a constant value up to 40°–50° and then gradually increases. The relative diffuse reflectances, R^{rel}_{diff}, measured on some modules, are reported as a function of the incidence angle in Fig. 12. Only modules with flat glass surfaces, and dot-like specular spots, were considered for this purpose. This is because it was only for these types of modules that the extraction of the specular spot from the sphere was possible at the different incidence angles. The curves in Fig. 12 reveal two different behaviours: the modules with ARC show low and scattered R^{rel}_{diff} values, whereas those without ARC show monotonically decreasing R^{rel}_{diff} values. The regular behaviour of $R^{rel}_{diff}(\theta)$ when ARC is absent can be explained considering that the specular reflection from the glass surface increases, following Fresnel, at increasing θ values and then the diffuse component of reflection from the silicon surface is overcome by the specular one at increasing incidence angles. The different behaviour of the $R^{rel}_{diff}(\theta)$ curves when ARC is present could be due to the superposition of interference effects from the ARC.

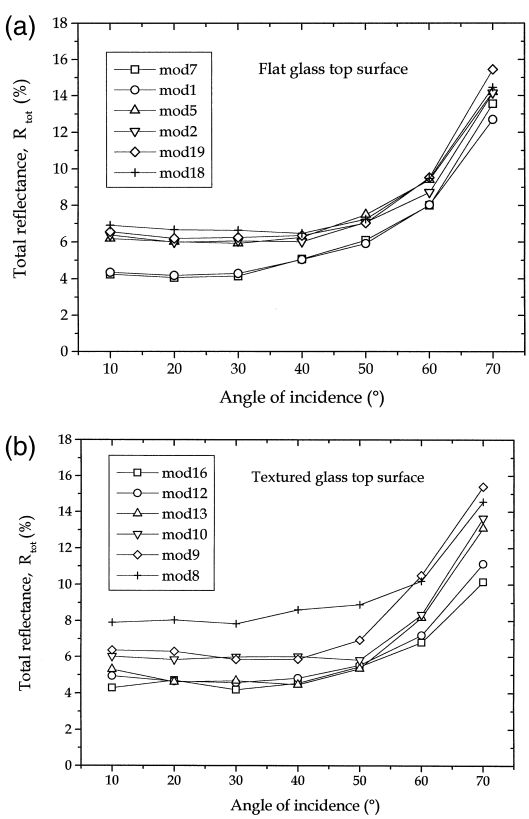

Fig. 11. (a) Total reflection curves, $R_{tot}(\theta)$, obtained for modules with a flat glass top surface. (b) Total reflection curves, $R_{tot}(\theta)$, obtained for modules with a textured glass top surface.

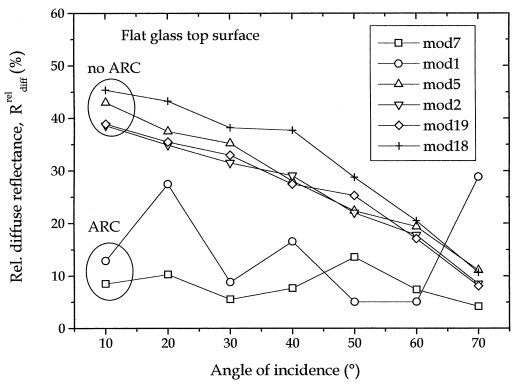

Fig. 12. Relative diffuse reflectance curves, $R^{rel}_{diff}(\theta)$, obtained for modules with flat glass surface. A different behaviour is found between modules with ARC and modules without ARC.

The transmittance of the module's cover can be expressed as:

$$T_{tot}(\theta) = 100 - R_{tot}(\theta) - A_{tot}(\theta)\,(\%), \tag{5}$$

where $A_{tot}(\theta)$ is the total absorbance of the glass sheet, here considered to be negligible, for simplicity. $T_{tot}(\theta)$ is the ability of the module's cover to transmit a light beam, inclined at an angle θ with respect to the normal, to the optically active layers of the cell. To study the relative optical losses in outdoor conditions [6,7], we introduce the transmittance factor $\tau(\theta)$:

$$\tau(\theta) = 100\,T_{tot}(\theta)/T_{tot}(0°)\,(\%). \tag{6}$$

The factor $\tau(\theta)$ expresses the ability of the module's cover to transmit inclined light beams at an angle θ, with respect to the normal incidence (STC conditions). The ability of the module to collect light at normal incidence is expressed by $T_{tot}(0°)$. In this work we use the transmittance at $\theta = 10°$, instead of $T_{tot}(0°)$ which could not be measured. The factor $\tau(\theta)$ is a key parameter in the calculation of the reflectance of a PV module at diffuse light, as it enters in the numerical routine [8] which is used to calculate the light transmitted to the module, taking into account each elemental ray of the sky hemisphere.

The $\tau(\theta)$ curves of some tested modules for flat and textured glass top surface are shown in Fig. 13a and b, respectively. By comparing Fig. 13a and b with Fig. 11a and b, it is evident that the less reflective modules at near-normal incidence are not necessarily the best for collecting inclined light beams, and vice versa. Module 7, for example, has a very low reflectance ($\sim 4\%$) at low angles, but it is the less efficient for collecting inclined light. The first reason for this result is because of the flatness of its glass and silicon surfaces. The second reason is because, since the total reflection is mostly due to the specular reflection from glass (thanks to the good antireflection effect of ARC), the module's reflection properties are mainly those of the air/glass interface ($n \approx 1.5$). As

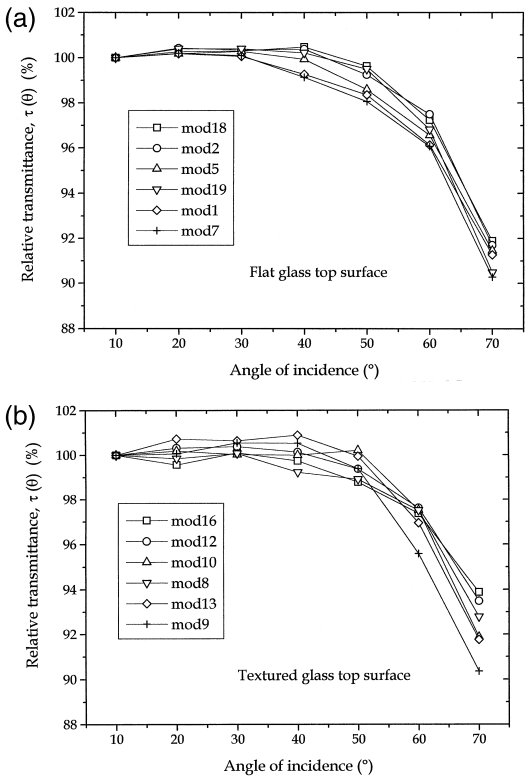

Fig. 13. (a) Relative transmittance curves, $\tau(\theta)$, obtained for modules with flat glass top surface. (b) Relative transmittance curves, $\tau(\theta)$, obtained for modules with textured glass top surface.

we will see in Section 3.2, this interface gives the highest reflection loss relative to the normal incidence. The $\tau(\theta)$ curves drop, on the average, after 40° for flat glass and after 50° for textured glass. The curves remain a little higher for the textured glass modules than for the flat glass modules. It comes out, therefore, that the glass texturization favours the collection of inclined light and then it plays a role similar to that of the ARC for the collection of light at normal incidence.

3.2. Comparison between theoretical and experimental $\tau(\theta)$ curves

To verify if the module can be modeled in a very simplified way, that is as a homogeneous, and semi-infinite, dielectric with an equivalent refractive index n_{eq}, we compare the $\tau(\theta)$ curves, obtained by applying the Fresnel equations, with the experimental ones obtained from the reflectance measurements on the mono-Si modules. Fig. 14 shows the theoretical curves of $\tau(\theta)$ calculated for a dielectric at five different values of the equivalent refractive index, in the interval 1.5–3.5. As observed by us in previous works [6,7], the $n_{eq} = 1.5$ and $n_{eq} = 2.0$ curves are very close, but also the curve for $n_{eq} = 2.5$ is

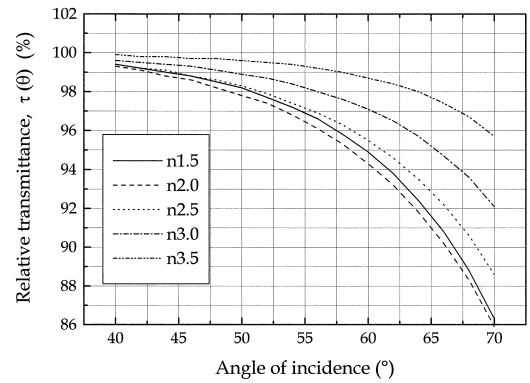

Fig. 14. Relative transmittance curves, $\tau(\theta)$, calculated for an air/dielectric interface at different refractive indices, n_{eq}, of the dielectric.

quite close to the $n_{eq} = 1.5$ curve, this last one representing a flat air/glass interface. The curves for $n_{eq} = 3.0$ and $n_{eq} = 3.5$ increasingly diverge from that at $n_{eq} = 1.5$. The curves of Fig. 14 are shown from 40° since they diverge significantly only starting from this incident angle. They are shown up to 75° because they will be compared to the experimental curves, which have a limit at $\theta = 70°$. The experimental curves of $\tau(\theta)$ were obtained for 17 of the 21 tested modules (see Table 3). By comparing the experimental and theoretical curves of $\tau(\theta)$, we obtained the values of n_{eq} as reported in Table 3. Almost all the values of n_{eq} vary in the interval 2.5–3.0, with the exception of module 6 which shows $n_{eq} = 3.5$. By comparing Table 2 with Table 3, it comes out that a lower value of n_{eq} corresponds to a lower total reflectance at 10°. By averaging the $\tau(\theta)$ values relative to the same category, that is

Table 3
Equivalent refractive indices of the mono-Si modules, obtained by comparing the theoretical and experimental $\tau(\theta)$ curves

Module	n_{eq}	Category
1	2.5	B
2	3.0	A
3	2.5–3.0	A
5	3.0	A
6	3.5	D
7	2.5	C
8	3.0	E
9	2.5–3.0	D
10	3.0	D
11	3.0	D
12	3.0	E
13	3.0	F
16	3.0	E
18	3.0	A
19	2.5–3.0	A
20	3.0	A
21	3.0	A

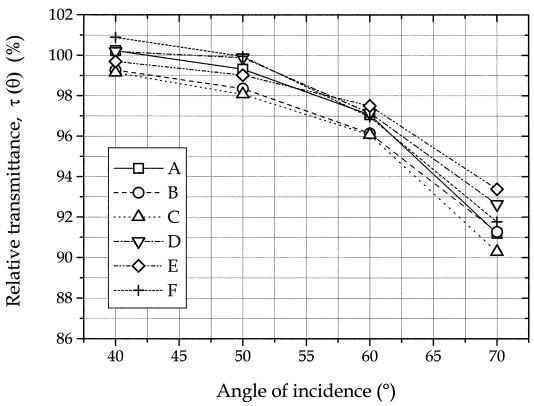

Fig. 15. Experimental curves of $\tau(\theta)$ for the six categories of modules. Each curve was obtained by averaging the $\tau(\theta)$ curves of modules belonging to the same category.

the same front structure, we obtain the six curves as shown in Fig. 15. By comparing Fig. 14 with Fig. 15, the average equivalent refractive index is obtained for each category of modules and reported in Table 1.

These results, which describe the transmittance properties of the modules' front covers, relative to STC, have been obtained on both isotropic and non-isotropic modules. They show that the modules can be modeled in a simplified picture as homogeneous dielectrics of refractive index varying between 2.5 and 3.0. These results seem to be in contrast with previous models [4,8,11] based on the assumption that the air/glass interface (with $n_{glass} = 1.5$) is the best optical model of the air/PV module interface, with respect to the STC conditions. In reality, the difference between the $n_{eq} = 1.5$ and the $n_{eq} = 2.5$ curves is not large, and then, for the modules of B and C categories (see Table 1), our model does not contrast significantly with the previous ones. Our investigation, moreover, brings to the result that textured glass modules, besides flat glass modules without ARC, can be modeled as flat, homogeneous dielectrics, with an equivalent refractive index, n_{eq}, of about 3.0. The peculiarity of the modules of category A, tested by us, is that they all have a flat glass surface also at the back (see Table 2).

We can conclude, therefore, our investigation on the PV modules' modeling by affirming, as far as conditions relative to STC are considered, that:

(i) modules with flat glass on top, and with ARC, could be modeled as dielectrics with $n_{eq} = 2.5$, or, as a good approximation, as just glass ($n_{eq} = 1.5$);

(ii) modules with flat glass on both sides, and no ARC, and modules with textured glass on top could be modeled as dielectrics with $n_{eq} = 3.0$.

3.3. Definition of light collection efficiency factor

To better investigate the relationship between the collection of inclined light and the structure of the module's front cover, we introduce the quantity f_{IL}, called 'light collection factor for inclined light relative to the normal incidence':

$$f_{IL} = 100 \times 2/\pi \times \int_{\theta=0}^{\theta=\pi/2} \tau(\theta)\,\mathrm{d}\theta \quad (\%), \tag{7}$$

This factor is not of immediate use for the calculation of the optical losses, but it is a means to quantify the closeness of the $\tau(\theta)$ curve to the 100% value in the 0–90° interval. Modules with $f_{IL} = 100\%$ should efficiently collect inclined light beams as at normal incidence, apart from a cos θ factor which establishes the total amount of energy from a parallel light beam incident on the module's surface at the angle θ.

The light collection factor f_{IL} has been calculated for most of the tested modules by numerical integration of the seven $\tau(\theta) = T_{tot}(\theta)/T_{tot}(10°)$ values:

$$f_{IL} = 100/9 \times \left[0.5 + \sum_{\theta_i = 10°}^{60°} \tau(\theta_i) + 1.5\tau(70°)\right] (\%), \tag{8}$$

The factor f_{IL} is reported versus $T_{tot}(10°)$ in Fig. 16. This figure, therefore, correlates the ability of the module to collect light at near-normal incidence to its ability to collect inclined light in the 0–90° interval, with respect to the near-normal incidence. Looking at the symbols of Fig. 16, it is possible to observe that a correlation between the structure of the module's front cover and the light collection factor f_{IL} exists. First of all, the modules with textured glass tops show the highest values of f_{IL}; intermediate values are obtained for the flat-glass/text-Si structures and the lowest values for the flat-glass/ARC/flat-Si and flat-glass/ARC/text-Si structures. Texturization of the glass surface, therefore, seems important for a better collection of inclined light beams, relative to the normal incidence, whereas texturization of the silicon surface plays

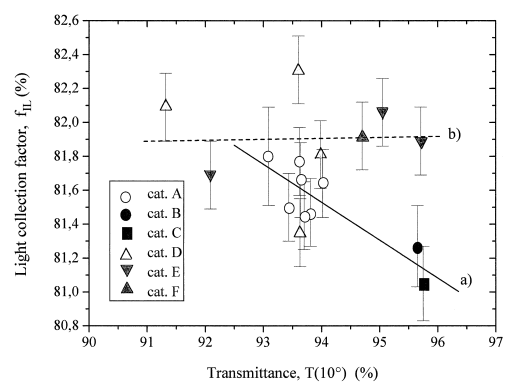

Fig. 16. Light collection factor, f_{IL}, calculated for the tested modules of Table 3, as a function of the transmittance at 10°, T (10°). Every point is indicated with a symbol correspondent to the module category. (a) Best fit for flat glass modules. (b) Best fit for textured glass modules.

a minor role for this purpose. The best combination, for a good collection of both normal incidence and inclined light, seems to be the structure of categories E and F (see Table 1): text-glass/ARC/flat-Si and text-glass/ARC/text-Si. From our investigation, it comes out clearly that the best module for light collection at near-normal incidence is not necessarily the best for the collection of inclined light relative to that at normal incidence. If the points of Fig. 16 are grouped as textured-glass top modules and flat-glass top modules, a very interesting behaviour emerges. The textured glass modules show high f_{IL} values, roughly constant with respect to $T_{tot}(10°)$ variations. The flat glass modules, on the contrary, show a decreasing behaviour of f_{IL} with increasing values of $T_{tot}(10°)$. This is shown in Fig. 16 by drawing two best-fit lines for the two groups of modules. The reason for that is comprehensible. The textured glass on the top 'captures' the inclined beams a little more efficiently and then the factor f_{IL} is less sensitive to the structure and reflection properties of the internal interfaces. As a consequence of this, all the textured glass modules show a similar value of f_{IL}. The flat glass modules have the air/glass interface which is a bad collector of inclined light. Modules with the highest values of $T_{tot}(10°)$ are also those whose reflection properties depend mainly on that interface. They show, therefore, the lowest values of f_{IL}. On the contrary, flat glass modules with low $T_{tot}(10°)$ values, reflect light also from the internal interfaces which are rougher than the flat glass and then can better collect inclined light. This explains why modules of category A show high values of f_{IL}, whereas modules of category B and C show low values of f_{IL}. Fig. 16 shows that the tested modules differ slightly in terms of f_{IL} ($< 2\%$) but sensibly ($\approx 5\%$) in terms of $T_{tot}(10°)$.

The use of a fixed angle of azimuth of the light's incidence plane, in our reflectance measurements, is not a limit for isotropic modules, in the sense that the reported results of reflectance can be fully extended to any other azimuth angle. For these modules, therefore, the reported reflectance values can be applied to calculate their optical losses, absolute or relative to STC conditions, for both the direct and the diffuse components of the skylight [6–8]. For anisotropic modules (textured-Si), the reported results apply well to the direct component of sunlight if the module is oriented with one of its main axes towards the South and at a tilt angle equal to the latitude. They can be applied, even though with a certain approximation, also to the calculation of the optical losses from diffuse light irradiation.

3.4. Spectral measurements

The spectral reflectance measurements of six modules, representing the six tested categories, are shown in Fig. 17. The modules with ARC (1, 7, 12, 13) show a well defined behaviour of $R_{tot}(\lambda)$ (decreasing values at increasing wavelengths), as a consequence of the interference effect produced by the ARC. This effect is very evident in module 7. Modules without ARC (2, 6) show, on the contrary, increasing values of $R_{tot}(\lambda)$ in the low wavelengths region. The lowest reflectances, in the entire spectrum, are obtained for modules 1 and 7 (categories B and C, respectively, the same which showed the lowest values of n_{eq}).

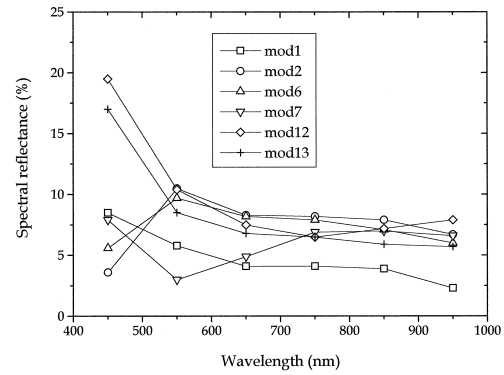

Fig. 17. Spectral total reflectance of the six module categories.

The reflectance values reported in Fig. 17 were not corrected for the effect of the grid, and then are a little higher than the values corresponding to the semiconductor area.

4. Summary and conclusions

We have presented a non-destructive method suitable for the measurements of a variety of optical properties of solar materials, solar cells and PV modules [12–14]. In this paper, we focused our attention on reflectance measurements made on mono-Si PV modules. The method does not require the cutting up of the PV modules. By using an integrating sphere apparatus, we were able to measure, for the first time, with a precision generally better than 5%, the reflectance of different types of PV modules. We used the monochromatic light of a laser, operating at $\lambda = 632.8$ nm, inclined at different incidence angles, from 10° to 70°. A well collimated laser beam, in fact, could be focused between two fingers of the solar cells, avoiding thus the collection of the light reflected from the grid. Spectral reflectance measurements were also made at 10°. We found that the optical properties of the modules improved in the latest manufactured modules. The knowledge of the absolute reflectance properties are important for improving their light collection capabilities and thus their output electric energy. For this purpose, we established that, independently from other features of the module, the presence of the ARC is fundamental to assure a low absolute reflectance, that is 4–5% at near-normal incidence. Modules without ARC showed total reflectances in the range of

6–9%. In this respect, a difference of about 5% in the efficiency of light collection exists between the best and worst modules at near normal incidence of light. The knowledge of the reflectance properties relative to the normal incidence is important for calculating the optical losses of PV modules relative to STC conditions [6,7] and, also, for selecting the most suitable modules for collecting diffuse light (this aspect is particularly important for the countries of northern Europe [15] or for installations of the modules on façades). We found that the modules are more similar among them with respect to the collection capability of inclined light, than with respect to the collection of normal incident light. The efficiency factor, f_{IL}, which we introduced to quantify the module's ability to collect inclined light beams, in fact, moves from 81% for the worst modules to about 82–83% for the best ones, with a difference smaller than 2%. We verified that this small difference is dependent mainly on the glass top surface roughness.

The decision about what type of module to install in a particular site is not straightforward, by looking at Fig. 16. The precise knowledge of the average direct and diffuse radiations of the site and that of the outdoor orientation of the module, combined with the data of optical losses (reflectance curves) are necessary to calculate, by using the method reported in Refs. [6,7], the final energetic loss produced by the optical (reflectance) effects.

We found also that the tested mono-Si modules, with respect to the STC conditions, could be optically modeled as homogeneous, semi-infinite dielectrics with an equivalent refractive index in the range 2.5–3.0, higher than that of the glass (1.5), as already suggested by us in previous works [6,7]. We have found a correlation between the value of n_{eq} and the structure of the module: (a) modules with flat glass and ARC can be modeled as $n_{eq} = 2.5$ dielectrics; (b) modules with a textured glass surface, or with a flat glass surface on both sides and no ARC, can be modeled as $n_{eq} = 3.0$ dielectrics. The modules of point (a) could further be approximated by a dielectric with $n_{eq} = 1.5$ (glass). This is because the $n_{eq} = 1.5$ and the $n_{eq} = 2.5$ theoretical curves are quite close. Our optical models have been derived by reflectance measurements performed on about 20 PV modules, limited to 70° incident angle and to a wavelength of 633 nm.

Acknowledgements

We want to thank Sergio Pietruccioli and Roberto Peruzzi (Eurosolare), Franco Traversa (Helios Technology) for the helpful discussions we had on PV modules technology. We also acknowledge Augusto Maccari for the discussions on the principles and practice of integrating spheres. We also want to thank Riccardo Schioppo and Antonio Romano for their assistance on the experimental work. Dr. Haruna Yakubu undertook this work with the support of the 'ICTP Programme for Training and Research in Italian Laboratories, Trieste, Italy'. This work was done with the financial support of the Italian Ministry of University and Technological Research (MURST).

References

[1] K. Bucher, Proc. 13th EC Photovoltaic Solar Energy Conference, H.S. Stephens & Associates, 1995, p. 2097.
[2] H. Gabler, M. Raetz, E. Wiemken, Proc. 12th EC Photovoltaic Solar Energy Conference, H.S. Stephens & Associates, 1994, p. 879.
[3] IEC Standards 891 and 1215, Bureau Central de la Commission Electrotechnique Internationale, Geneva.
[4] R. Preu, G. Kleiss, K. Reiche, K. Bucher, Proc. 13th EC Photovoltaic Solar Energy Conference, H.S. Stephens & Associates, 1995, p. 1465.
[5] S. Lanzerstorfer, G. Bauer, H. Wilk, Proc. 13th EC Photovoltaic Solar Energy Conference, H.S. Stephens & Associates, 1995, p. 2294.
[6] A. Parretta, A. Sarno, R. Schioppo, M. Zingarelli, L. Vicari, Proc. 14th EC Photovoltaic Solar Energy Conference, H.S. Stephens & Associates, 1997, p. 242.
[7] A. Parretta, A. Sarno, L. Vicari, Effects of solar irradiation conditions on the outdoor performance of photovoltaic modules, Optics Commun. 153 (1998) 153–163.
[8] S. Li Causi, C. Messana, G. Noviello, A. Parretta, A. Sarno, Proc. 13th EC Photovoltaic Solar Energy Conference, H.S. Stephens & Associates, 1995, p. 1469.
[9] S. Krauter, R. Hanitsch, P. Campbell, S.R. Wenham, Proc. 12th EC Photovoltaic Solar Energy Conference, H.S. Stephens & Associates, 1994, p. 1198.
[10] ASTM E 1175-87, Standard Test Method for Determining Solar or Photopic Reflectance, Transmittance and Absorptance of Materials Using a Large Diameter Integrating Sphere, American Society for Testing and Materials, PA, USA, 1987 (also reapproved, 1996).
[11] E.A. Sjerps-Koomen, E.A. Alsema, W.C. Turkenburg, Solar Energy 57 (1996) 421.
[12] Patent It. a.n. RM 97A000676, 5 November 1997.
[13] A. Parretta, A. Sarno, H. Yakubu, A Novel Apparatus for the Optical Characterization of Solar Cells and Photovoltaic Modules, presented at the 2nd World Conference and Exhibition on Photovoltaic Solar Energy Conversion, Vienna, Austria, 6–10 July 1998 (in press).
[14] A. Parretta, A. Sarno, M. Pellegrino, C. Privato, E. Terzini, A. Romano, H. Yakubu, Optical Reflectance Mapping (ORM): A Diagnostic Tool in the Study of Light Collection in PV Modules, presented at the 2nd World Conference and Exhibition on Photovoltaic Solar Energy Conversion, Vienna, Austria, 6–10 July 1998 (in press).
[15] N.B. Mason, T.M. Bruton, K.C. Heasman, Proceedings 12th German National PV Solar ENERGY Symposium, OTTI Regensberg, 1997, p. 383.
[16] S.R. Wenham, M.A. Green, M.E. Watt, Applied Photovoltaics, Centre for Photovoltaic Devices and Systems, 1977, p. 79.
[17] A. Maccari, M. Montecchi, F. Treppo, M. Zinzi, CATRAM, An apparatus for the optical characterization of advanced transparent materials, Appl. Opt. 37 (1998) 5156.